Micro- and Nanostructured Surface Morphology on Electrospun Polymer Fibers

ARTICLE *in* MACROMOLECULES · OCTOBER 2002

Impact Factor: 5.8 · DOI: 10.1021/ma020444a

Micro- and Nanostructured Surface Morphology on Electrospun Polymer Fibers

Silke Megelski,[†] Jean S. Stephens,[†] D. Bruce Chase,[‡] and John F. Rabolt*[,†]

Department of Material Science and Engineering and Delaware Biotechnology Institute, University of Delaware, Newark, Delaware 19716; and Central Research and Development, Experimental Station, Dupont, Wilmington, Delaware 19880

Received March 21, 2002

ABSTRACT: Electrospun fibers were produced using a variety of solvents to investigate the influence of polymer/solvent properties on the fiber surface morphology. Electrospinning is a novel processing technique for the production of fibers with diameters in the range of a few nanometers to tens of micrometers. We have been able to produce polymeric fibers with a high surface area through the introduction of a micro- and nanostructured surface structure, which we refer to as a "porous" morphology. These features could be introduced in several different polymeric fibers increasing their range of application significantly. The pores vary from densely packed, well-formed nanopores with diameters in the range 20−350 nm to larger flat pores of about 1 μm. The increased surface area of polymeric fibers was correlated with high volatility solvents used in the electrospinning process. The effect of processing parameters on the fiber surface morphology was also investigated using optical microscopy, field emission scanning electron microscopy (FESEM), transmission electron microscopy (TEM), and atomic force microscopy (AFM).

Introduction

The ability to shape materials on different length scales including the nanoscale is important for many applications. When high surface-to-volume ratio materials are required, nanoparticles are often the first choice, but introducing nanoscale texture/features on nano- or microsized materials will also further increase the surface-to-volume ratio.

Spontaneously assembled submicron structures have been described previously in a variety of material systems. Recently Srinivasarao et al. reported the formation of a three-dimensionally ordered array of air bubbles in a polystyrene (PS) film based on evaporative cooling and the formation of breath figures.[1] Porous PS membranes have also been created by a thermally induced phase separation (TIPS) technique.[2,3] Porous membranes from different polymeric materials have been prepared by other phase separation techniques, but also recently by electrospinning polymers onto a grounded target to create a mat.[4−6] Nanoscale structures on electrospun polymer fibers of poly-L-lactide (PLLA), polycarbonate (PC), and poly(vinylcarbazole) fibers using dichloromethane as a solvent were briefly described by Bognitzki et al.[7] Recently they reported the preparation of nanostructured polylactide (PLA) and poly(vinylpyrrolidone) (PVP) fibers by selective removal of one of the polymer phases after electrospinning the fibers from a ternary solution.[8]

Traditional melt spun fibers range in diameter from about 5 to 200 μm, whereas electrospun fibers can have diameters in the nanometer range.[9−11] Electrospinning of a variety of synthetic as well as natural polymer fibers for different applications has also been reported in the literature.[7,9,12−21] Electrospinning, derived from electrospraying,[22,23] employs a pipet or syringe and needle that contains a polymer solution which can be charged by an electrode hanging in the solution or by a high voltage applied to a needle at the end of the syringe. A polymer droplet suspended from the end of the needle becomes deformed from a hemispherical shape to a conical shape, called a Taylor cone, by electrical forces. When the accumulated charge on the surface of the droplet overcomes the surface tension, a polymer jet is ejected from the tip of the cone. The jet reaches an instability point after a few centimeters of travel from its origin and the jet begins to whip or splits into bundles of smaller fibers. There are a number of works describing the electrically forced jet and its instabilities.[24−29] The electrospun fibers are then collected on an oppositely charged or grounded target, producing a macroscopically isotropically oriented fiber mat. Recently, Theron and co-workers have demonstrated the collection of aligned fibers on a rotating disk.[30]

The goal of this work is to investigate the different polymer/solvent systems in which micro- and nanopores can be produced on electrospun fiber surfaces. By varying polymer architecture and processing parameters, polymeric fibers can be spun with a large surface area for different applications such as membranes for special textiles, filter systems, biological sensors, scaffolds, and transport media. The influence of the material characteristics and the processing parameters on the surface morphology of electrospun fibers was investigated using several techniques, including optical microscopy, FESEM, TEM, and AFM. Our studies have concentrated on the micro- and nanostructured surface morphology as a function of solution concentration, spinning voltage, flow rate of the solution, and the needle to target distance (working distance). A variety of crystalline and amorphous polymers, including polycarbonate (PC), poly(ethylene oxide) (PEO), and poly(methyl methacrylate) (PMMA), were electrospun from different solvent systems to compare their surface morphology. In addition the influence of solvent vapor pressure was investigated on electrospun PS in detail.

* To whom correspondence should be addressed. E-mail: rabolt@UDEL.edu.
[†] University of Delaware.
[‡] Dupont.

10.1021/ma020444a CCC: $22.00
Published on Web 09/27/2002

Table 1. Polymer Data

polymer	T_g (°C)	T_m (°C)	M_w (g mol^{-1})	ϵ_r/1 kHz	ρ (g cm^{-3})
PS	100	240	190 000	2.4−2.65	1.04
PC	150	265	60 000	3.0 (25 °C)	1.20
PMMA	105		540 000	3.0−3.6	1.20
PEO	−67	65	300 000		1.21

Experimental Section

Materials. To prepare electrospun fibers of PS, different weight concentrations (M_w = 190 000; Scientific Polymer Products) in tetrahydrofuran (THF) (HPLC; Fisher Scientific), dimethylformamide (DMF) (certified A.C.S.; Fisher Scientific), carbon disulfide (CS_2) (reagent A.C.S.; Fisher Scientific), and toluene (certified A.C.S.; Fisher Scientific) were used. Other polymer/solvent systems investigated were PEO (M_w = 300 000; BDH laboratory reagents) in water, chloroform ($CHCl_3$) (HPLC; Fisher Scientific), and acetone (HPLC; Fisher Scientific); PMMA (M_w = 540 000; Scientific Polymer Products) in THF, acetone, and $CHCl_3$; and PC (M_w = 60 000; Scientific Polymer Products) in $CHCl_3$ and THF. All the polymers, except PC, dissolved at room temperature with 1−2 h of stirring. PC dissolved in THF in a warm water bath after a minimum of 4 h of strong stirring. The properties of the polymers and solvents used are listed in Tables 1 and 2, respectively.

Electrospinning Experiments. A schematic of the electrospinning apparatus is shown in Figure 1. A polymer solution was placed in a 5 mL syringe attached to a syringe pump (Orion SAGE) in a vertical mount. The potential was applied to the hypodermic needle (Hamilton) on the end of the syringe using a high voltage power supply (Glassman High Voltage). A grounded aluminum sheet was placed on the surface of an adjustable lab jack and used as the target. The distance between the needle and target was optimized for each set of experiments. The spinning conditions for each polymer are listed in Table 3.

Characterization. Viscosity measurements of the polymer solutions were performed with a stress-controlled rheometer at 25 ± 0.1 °C (Rheometric SR 500). The diameter and morphology of the electrospun polymer fibers were determined by optical microscopy (Olympus BX60), field emission scanning electron microscopy (FESEM, JEOL JSM-6330F), and AFM (Nanoscope III, Digital Instruments). Since most electrospun fibers observed in these experiments do not have a round cross section but appear more ribbonlike, we will use the largest measurement of the aspect ratio (of a fiber cross section) as the diameter for comparison purposes. To obtain FESEM images the fibers were collected on an aluminum SEM disk then coated with carbon or gold. The acceleration voltages and the working distances for each image are stated in the figure captions. The cross sections of the fibers were determined using TEM (JEOL JEM 2000FX). For each sample a microtomed slice of fiber embedded in an epoxy resin placed on a copper grid was used. The fibers were stained before analysis in a RuO_4 atmosphere for 105 min, placed in epoxy resin (embedding kit DER 332−732; Electron Microscopy Science), and hardened in an oven at 45 °C for 14 h and then at 60 °C for 3 days.

Results

Varying Electrospinning Conditions. Electrospinning processing parameters (such as solution concentration, spinning voltage, working distance, and solution feeding rate) influence the morphology of the polymeric fibers as shown previously.[15,31] These parameters have been investigated in order to electrospin PS from THF and to find the optimum conditions for obtaining beadless fibers. Moreover the influence of these processing parameters on the surface morphology and pore formation on PS fibers have also been investigated and will be discussed below.

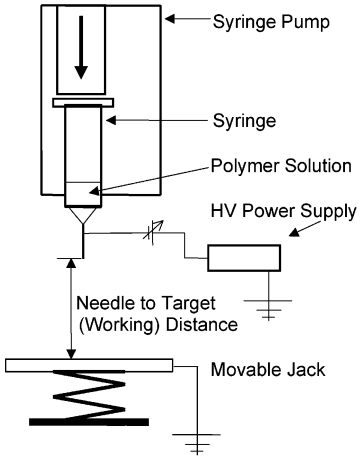

Figure 1. Schematic diagram of electrospinning apparatus.

A. Solution Concentration. The concentration of PS in THF was varied from 18 to 35 wt % in order to study its effect on the fiber morphology and pore formation. The viscosity of the solution increased as the PS concentration increased. All other spinning parameters were kept constant as shown in Table 4. Optical micrographs show an increase in fiber diameter from 0.8 to 20 (±10) μm with increasing solution concentration. The PS fibers are beaded up to a concentration of 30 wt % with the occurrence of beads decreasing with increasing solution viscosity. The size of the beads as well as the size of the fibers increases with higher PS concentration, as shown in Figure 2.

All PS fibers observed in this work have a ribbon-shaped cross section and a surface with nanoporous features, as shown by the FESEM images in Figure 3. The shape and the size of these nanopores were observed to change with concentration. The 18 wt % PS sample has two kinds of pores, smaller mostly rounded pores about 20 nm in diameter and larger elongated pores with dimensions of approximately 200 nm in the long axis direction (Figure 3a). The pores in fibers spun at higher PS concentrations are approximately round and have a narrower size distribution of 50−180 nm. At 25 wt % PS, the pores have a rounder shape and are about 50−100 nm in diameter. PS fibers spun from a 35 wt % solution display round pores that are somewhat overlapped with each other and have diameters that range from about 50 to 180 nm. Typically these fibers

Table 2. Solvent Data

solvent	T_b (°C)	T_m (°C)	p_v/25 °C (kPa)	ρ (g cm^{-3})	η/20 °C (mPa s)	ϵ/20 °C	c_p (J g^{-1} K^{-1})	μ (D)	γ/25 °C (mN m^{-1})
CS_2	46	−100	48.2	1.2632		2.6	1.00	0	31.58
acetone	56	−94	30.8	0.7899	0.324	20.7 (25 °C)	2.18	2.88	23.46
$CHCl_3$	62	−63.5	26.2	1.4832	0.568	4.806	0.96	1.04	26.67
THF	66	−108	21.6	0.8892	0.468	7.6	1.72	1.75	23.97 (?)
cyclohexane	81	7	13	0.7785	0.979	2.023	1.84	0	24.65
water	100	0	2.3388	0.998 23	1	78.54	1.00	1.84	71.99
toluene	111	−95	3.79	0.8669	0.59	2.379 (25 °C)	1.70	0.37	27.93
DMF	153	−61	2.7	0.944 (25 °C)	0.92	36.7	2.06	3.82	

Table 3. Conditions for Electrospinning

polymer	M_w (g/mol)	solvent	c (wt %)	U (kV)	d (cm)	flow rate (mL/min)	needle o.d. (mm)	fiber o.d./pore o.d. (μm/nm)
PS	190 000	CS_2	30	20	12	0.10	0.35	4−25/<100−750
		THF	18−35	10	35	0.07	0.51	5−15/50−150
		acetone/cyclohexane	30	10	35	0.07	0.51	15−30/300−1000
		toluene	30	14	15	0.07	0.16	∼5/no pores
		DMF	30	10	35	0.07	0.51	∼10/no pores
		THF/DMF	30	10	35	0.07	0.51	∼10/50-
PEO	300 000	H_2O	10	7	15	0.0025	0.51	0.2−0.8/no pores
		$CHCl_3$	10	8	25	0.19	0.51	∼10/no pores
		acetone	10	8	20	0.24	0.51	0.8−14/no pores
PC	60 000	$CHCl_3$	20	10	35	0.09	0.51	10−12/100−250
		THF	20	10	35	0.07	0.35	∼20/micropores
PMMA	540 000	THF	10	10	35	0.07	0.51	10−35/micropores
		acetone	10	10	35	0.07	0.51	∼7.5/∼250
		$CHCl_3$	10	10	35	0.09	0.51	0.75−13/75−250

Table 4. Processing Parameter of Electrospinning PS from THF

c (wt %)	viscosity (Pa s)	U (kV)	d (cm)	flow rate (mL/min)	needle o.d. (mm)
18	0.085	10	35	0.07	0.51
20	0.116				
25	0.214				
28	0.258				
30	0.360				
35	0.614				
35	0.614	5	35	0.07	0.51
		7.5			
		10			
		12			
35	0.614	10	30	0.07	0.51
			25		
			20		
			15		
35	0.614	10	35	0.004	0.51
				0.07	
				0.10	
				0.14	
				0.24	

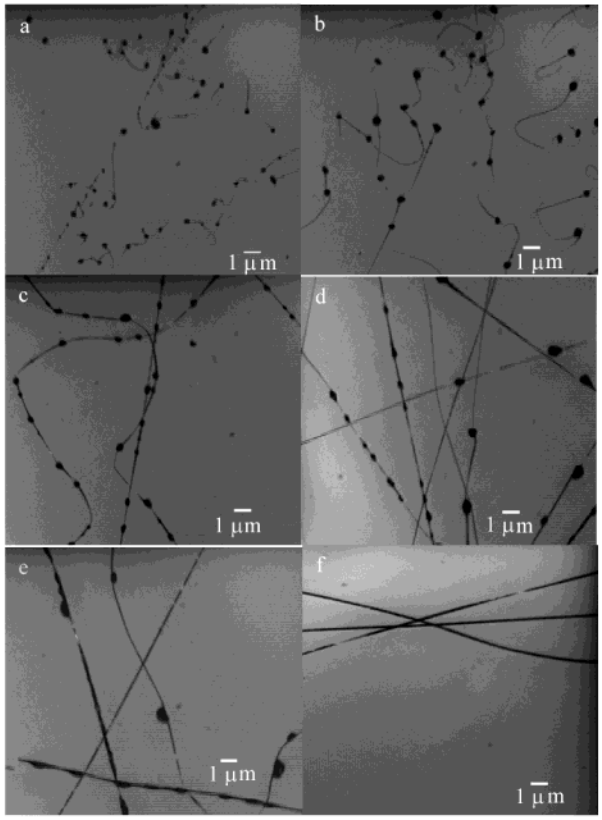

Figure 2. Optical microscope images (5× enlargement) of PS fibers electrospun from THF as a function of PS concentration: (a) 18 wt %; (b) 20 wt %; (c) 25 wt %; (d) 28 wt %; (e) 30 wt %; (f) 35 wt %.

are twisted as shown in Figure 3e. Figure 3f shows a high contrast FESEM micrograph, which represents the microtexture of the fiber surface.

B. Spinning Voltage. The voltage applied during electrospinning was also varied and its influence on the PS fibers investigated. The fiber size decreases from about 20 to 10 μm with increasing spinning voltage (5−12 kV), keeping all other conditions constant. The PS fibers have a ribbon-shaped cross section and are twisted. Some beads occur, but only at 5 and 12 kV. In addition, the surfaces of these PS fibers are rough, and nanopores with pore diameters in the range 50−350 nm appear to be densely packed on the surface. The pore size distribution is not affected by changing the voltage. A TEM image, shown in Figure 4, of a PS fiber cross section spun at 7.5 kV confirms the ribbon shape of the fiber and the roughened surface with densely packed nanopores. The double bonds of the phenyl ring on the PS fiber surface combine with RuO_4 and appear as dark areas in the TEM due to their higher scattering capacity for electrons. It is very clear that these pores are located only on the fiber surface and have a depth of about 50−75 nm, which has also been independently verified by AFM.

C. Working Distance. To assess the effect of working distance on fiber morphology, the gap between the highly charged needle and the grounded target was narrowed from 35 to 15 cm in 5 cm steps, keeping all other parameters constant. It was found that, although the fiber size does not change significantly, inhomogeneously distributed elongated beads start to form along the PS fibers after reducing the working distance by only 5 cm. The morphology of the ribbon-shaped PS fibers is also not influenced by changing the working distance. All fibers have microstructure textured surfaces and nanopores, which range in size from 70 to 200 nm in diameter.

D. Flow Rate. The pump speed and hence the flow rate of the PS solution was changed to determine its effect on fiber size and morphology. Bead formation is observed when the flow rate is 0.10 mL/min and higher. The ribbon-shaped fibers increase in size from about 5 to 20 μm and show the typical microtexture and nanopores. The pore sizes range in diameter from 50 to 250 nm. The mean pore size is observed to increase from about 90 to 150 nm with increasing flow rate. In Figure 5 are shown the FESEM images of these fibers as a function of flow rate.

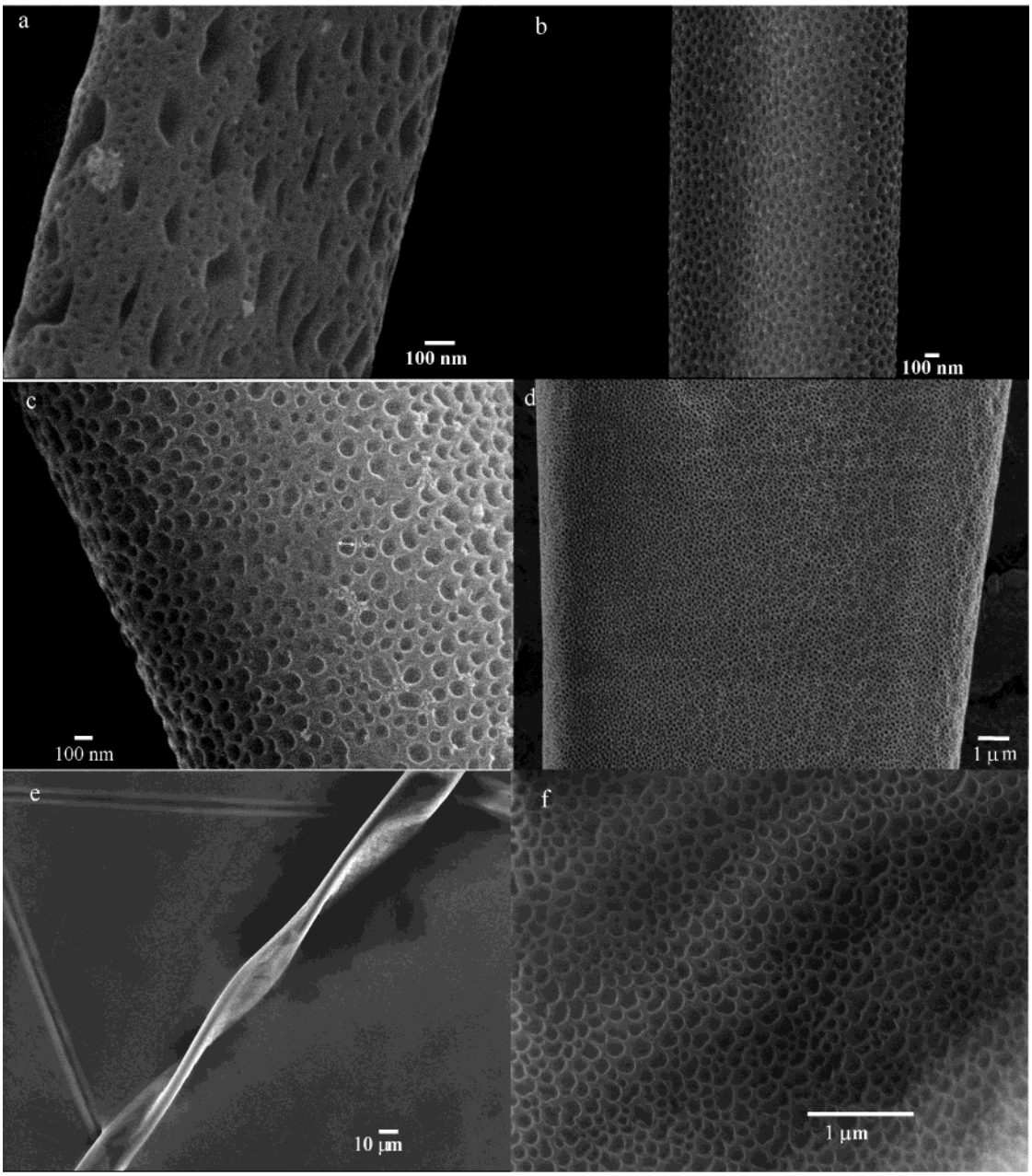

Figure 3. FESEM images of PS fibers electrospun from THF as a function of PS concentration: **(**a) 18 wt % (15 kV, WD 6.1 mm); (b) 25 wt % (15 kV, WD 5.8 mm); (c) 28 wt % (15 kV, WD 5.8 mm); (d) 30 wt % (2.0 kV, WD 8.6 mm); (e) 35 wt % (15 kV, WD 5.5 mm); (f) higher magnification of part e (15 kV, WD 5.5 mm).

The conditions to produce beadless ribbon-shaped fibers of PS electrospun from THF were found to be as follows: 30 to 35 wt % concentration, 7.5 to 10 kV, 35 cm working distance, and 0.07 mL/min flow rate. PS fibers electrospun under these conditions have diameters in the range of 20 ± 10 μm with a microtextured surface and densely packed nanopores with diameters in the 50−200 nm range. The bead formation is a function of the PS concentration as well as of the spinning voltage, the working distance, and the feed rate. A lower concentration or deviation of the voltage from the optimum as well as a smaller distance between needle and target or faster flow rate resulted in beaded fibers with different diameters. The size range of PS fibers produced in this work ranges from 0.8 to 20 (± 10) μm. An increasing solution concentration or increasing flow rate as well as a decrease in spinning voltage resulted in increased fiber size. The influence of these parameters on the pore formation is not as obvious as it is for bead formation and fiber size. The pores range in size from 20 to 350 nm. They vary in size and shape with changing PS concentration. There are even pores of differing size and shape in one PS fiber electrospun from THF (18 wt %).

Electrospinning PS from Varying Solvents. Although many synthetic and natural polymers have been electrospun using a variety of solvents, the formation of pores was briefly described only by Bognitzki et al.[7] Work has also appeared on PS membranes, where the pores are either a function of solvent density or are created by thermally induced phase separation techniques.[1−3] In this work, we believe that the physical properties of the solvents play an important role in this process and hypothesize that the solvent volatility plays a critical role in the pore formation process. Therefore, for comparison, a variety of solvents with different boiling

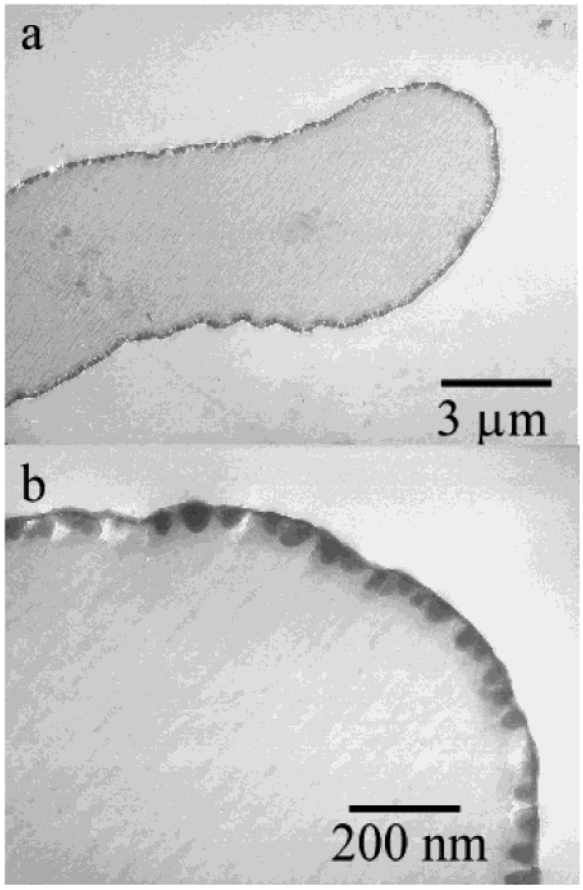

Figure 4. TEM image (2000 kV) of a cross section of a PS fiber electrospun from THF (35 wt %, 7.5 kV, 0.07 mL/min, 35 cm, 0.51 mm needle diameter).

points and vapor pressures (Table 2) were used to electrospin PS fibers.

A. Carbon Disulfide (CS_2). The most volatile solvent used was CS_2. Its vapor pressure was so high that the polymer droplet on the needle formed a skin on its surface almost immediately. Therefore, jet formation was only possible after renewing the droplet frequently. Electrospun fibers were created between large droplets (see conditions in Table 3) and were investigated with FESEM.

The fibers (4−25 μm in diameter) shown in Figure 6 also have a ribbon-shaped cross section and exhibit additional ribbonlike textures along the fibers. The surface of these fibers is smooth with pores ranging from about 100 to 750 nm that are not packed as densely as those observed on PS fibers spun from THF.

B. Toluene. It was more difficult to electrospin PS from toluene than from THF. With the conditions listed in Table 3, a small jet was formed for only a few seconds. The collected fibers were approximately 5 μm in diameter and were ribbon shaped. The fiber surface is very rough, showing no defined pores but rather large elongated holes of about 1 μm, primarily on the flat side of the fiber.

C. Tetrahydrofuran/Dimethylformamide (THF/DMF). In a more detailed experiment we investigated THF/DMF mixtures with solvent ratios of 90/10, 75/25, 50/50, 25/75, and 10/90%. Figure 7 shows the effect of the decreasing vapor pressure of the solvent mixture on the observed microtexture for PS fibers spun from 100% THF, THF/DMF ratios of 75/25 and 50/50%, and 100% DMF. Like PS electrospun from THF only, the fibers are ribbon shaped and are approximately 10 μm in diameter. At a ratio of 75/25% THF/DMF (Figure 7b) the pores become larger, less uniform, and shallower than those on fibers electrospun from 100% THF (Figure 7a). Surface roughness and/or microtexture is observed at 50/50% THF/DMF (Figure 7b), but these features disappear when the fibers are spun from 100% DMF (Figure 7d). The microtexture diminishes until it finally disappears, leaving a smooth surface with decreasing solvent volatility.

In general, a very high density of pores was observed on PS fibers electrospun from THF, and the resulting microtexture induced at the fiber surface increases the surface area by as much as 20 to 40% depending on the diameter of the fiber. The influence of the solvent vapor pressure could be observed by substitution of THF with DMF with the microtexture and nanopores of the PS fibers disappearing as the volatility of the mixed solvent system decreased. To be sure of the effect of solvent volatility, we have also investigated mixtures of acetone and cyclohexane to electrospin PS. These fibers showed an increase in surface roughness and pores with increasing boiling point of the solvent mixture. However, both solvents form an azeotrope at 67/33% with a lower boiling point of 53 °C, which makes an interpretation more complex.

Investigation of Different Polymers. In addition to PS, the influence of the solvent on electrospinning of other polymers was also investigated. The aim was to determine whether a large variety of porous polymer fibers with a tailorable surface morphology could be produced for different applications. The polymers included PMMA, PC, and PEO, and the electrospinning conditions used are listed in Table 3. The solution concentration was adjusted so that electrospinning could take place under almost identical instrument conditions for each polymer.

A. Atactic Poly(methyl methacrylate) (PMMA). PMMA is an amorphous polymer with high optical clarity making it important for applications where light transmission is necessary. It is also resistant to many aqueous-based inorganic reagents, including dilute alkalis and acids.[32] In this study, we investigated the surface morphology of PMMA fibers electrospun from acetone, $CHCl_3$, and THF, which are shown in Figure 8.

Like all electrospun PS fibers studied thus far, the PMMA fibers had a ribbon-shaped cross section independent of the solvent (acetone, $CHCl_3$, THF) used. Those fibers spun from the most volatile solvent, acetone, have a diameter of about 7.5 μm. The fiber surface contains a small amount of texture with some broadly distributed pores that were elongated along the fiber direction and were about 250 nm in size (Figure 8a). There was a bimodal distribution of fibers created during electrospinning PMMA from $CHCl_3$. The smaller fibers had a diameter of approximately 750 nm and were very beaded, whereas the larger fibers had a diameter of about 13 μm and appeared more uniform. No beads were present but the fibers did contain a microtextured surface distinctly different from that produced from acetone. Only the larger fibers exhibited very densely packed pores of about 75 to 250 nm (Figure 8, parts b and c). Fibers of about 10 μm in diameter with a microtextured surface morphology were observed for PMMA spun from THF (Figure 8d). This microtexture appeared as large flat pores of about 1 μm or larger.

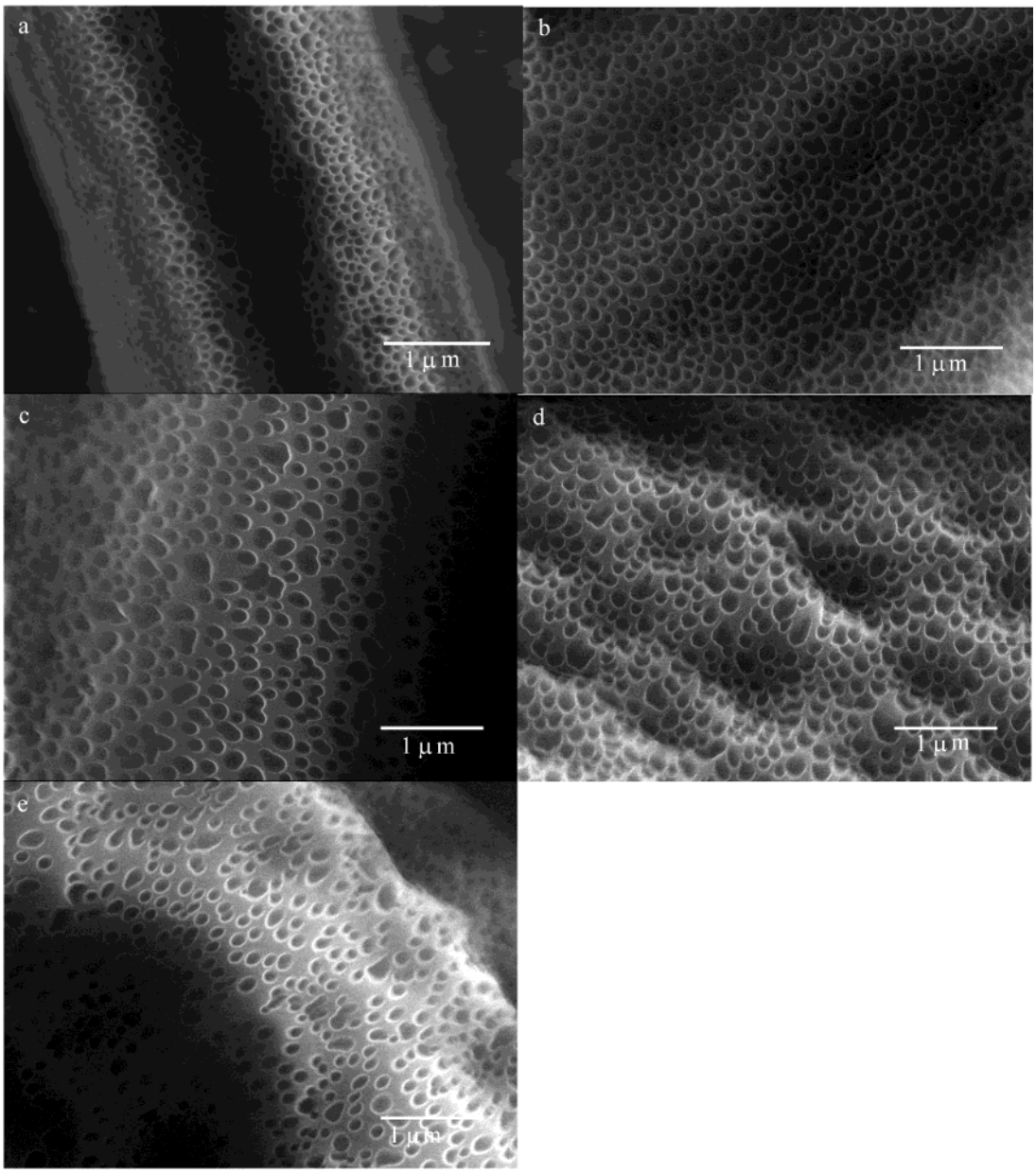

Figure 5. FESEM images of PS fibers as a function of flow rate: (a) 0.004 mL/min (5 kV, WD 9.5 mm); (b) 0.07 mL/min (15 kV, WD 5.5 mm); (c) 0.1 mL/min (15 kV, WD 5.2 mm); (d) 0.14 mL/min (15 kV, WD 5.5 mm); (e) 0.24 mL/min (15 kV, WD 5.5 mm).

PMMA electrospun from $CHCl_3$ produces fibers with the largest surface area and most distinctive pores therefore making $CHCl_3$ best solvent for producing a highly textured PMMA fiber (Figure 8). However, it seems that other factors in addition to vapor pressure must also be considered to explain the formation of surface textures and nanopores on electrospun polymer fibers.

B. Polycarbonate (PC). PC is a semicrystalline polymer with very good mechanical properties including high impact strength, good heat resistance and good thermal and oxidative stability in the melt. We have investigated the fiber formation of PC electrospun from $CHCl_3$ and THF to compare the surface morphology with that of PS and PMMA.

PC fibers spun from $CHCl_3$ have a diameter of about 10 μm with some observable texture in the flat part of the ribbon-shaped fibers. Round and slightly elongated nanopores of about 100−250 nm that are broadly distributed appeared on the fiber surface (Figure 9a). PC fibers formed from THF are also ribbon shaped but with a very pronounced microtexture, which can also be described as irregularly shaped micropores with diameters of approximately 20 μm. FESEM images of both fiber samples are shown in Figure 9.

C. Poly(ethylene oxide) (PEO). PEO is of great commercial interest, because it combines thermoplastic behavior and mechanical properties of a highly crystalline, high-molecular-weight polymer with complete water solubility.[32] Its use for synthetic fibers, thickeners, and stabilizers in different materials makes PEO a favorite choice for electrospinning as already illustrated by others.[27,31,33,34] The aim of our experiments was to determine the solvent effect on the PEO fiber surface morphology. When acetone, $CHCl_3$ and water are used as solvents, the electrospun fibers exhibit a round cross section in contrast to all the other polymer fibers studied thus far. The smallest PEO fibers were formed from aqueous solution and were about 200−800 nm in

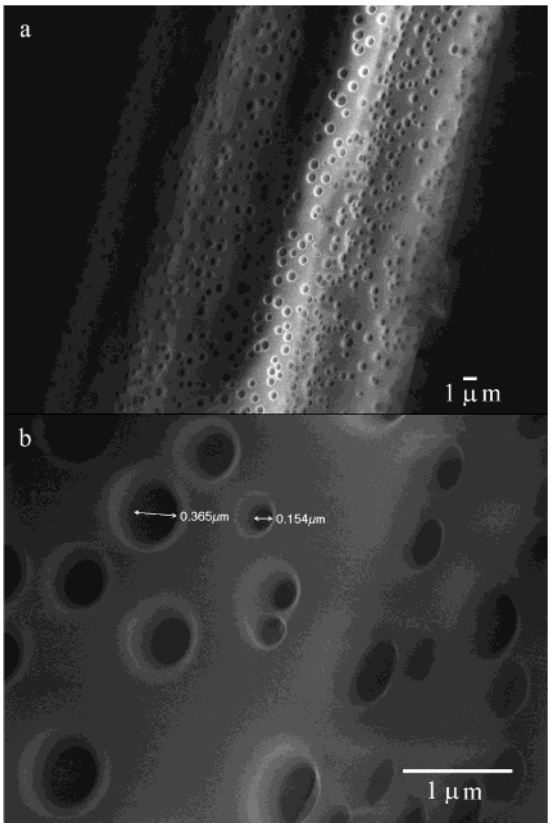

Figure 6. (a) FESEM image of PS fiber electrospun from CS_2 at 30 wt %; (b) higher magnification of part a (15 kV, WD 8.0 mm).

diameter. When PEO fibers were electrospun from acetone and $CHCl_3$ the fiber diameter varied from about 800 to 1400 nm. The surface of the fibers are smooth when electrospun from acetone and water, but they exhibit a slightly rough surface if electrospun from $CHCl_3$. Pores are not observed on any of these electrospun PEO fibers, even though in some cases they were electrospun from volatile solvents. Currently we do not have an explanation for this, but note that PEO has a quite different glass transition temperature, T_g, of −67 °C compared to PS (T_g = 100 °C), PMMA (T_g = 105 °C), and PC (T_g = 150 °C).

In general, a broad range of porous polymer fibers or fibers with large surface areas have been produced by electrospinning from several highly volatile solvents. Electrospun PMMA fibers from $CHCl_3$ and also from THF exhibit a nanoporous surface texture. As the boiling points of the solvents (acetone, $CHCl_3$, and THF) used to electrospin PMMA are very similar, it was not possible to determine their influence on the formation of surface microtextures and nanopores. It has also been shown that it is possible to form PC fibers with a very distinct microtexture from THF, whereas PC fibers electrospun from $CHCl_3$ showed a smooth fiber surface with nanopores present. In addition, electrospinning PEO from water, acetone, and $CHCl_3$ as well as electrospinning PS from THF at the lowest concentration could produce submicrometer fibers. However no nanopores were observed on electrospun PEO fibers under any processing conditions. When PEO was spun from $CHCl_3$, a slightly rough fiber surface was formed, and in contrast to all the other investigated materials, PEO fibers always had a round cross section.

Discussion

Electrospinning polymer solutions involves a rapid evaporation of the solvent while the jet is accelerated to the counter electrode.[35] Within milliseconds the surface area of the jet is increased dramatically. This could lead to a number of thermodynamically driven events. For example, a crossing of phase boundaries and a resulting structure formation by phase separation can occur as noted by Bognitzki and co-workers.[7] They postulate that this favors a spinodal phase separation, because nucleation phenomena require more time than the initial growth of unstable concentration fluctuations. Furthermore, the phase-separated regions would not have the time to coarsen strongly before vitrification. As a result they found that very fine phase morphologies are preserved and this leads to the following question: Why do these phase morphologies exist only on the surface of the electrospun fibers?

The formation of nano- and microstructures by phase separation in membrane preparation processes is very well-known and widely discussed in the literature.[4,5,36−39] There are different phase separation techniques such as immersion precipitation, air-casting of the polymer solution, vapor-induced phase separation, and thermally induced phase separation (TIPS). An understanding of these techniques may also help to explain the pore formation in electrospun fibers. In addition, evaporative cooling at the surface of the fibers could lead to the condensation of moisture and the formation of breath figures as discussed by Srinivasarao et al. It is clear that the electrospinning process is more complex since the fibers are carrying charge, which is not present in the formation of other porous structures.

If a polymer solution (polymer and solvent) is cast on a support, evaporation takes place under convective conditions. During solvent evaporation the solution becomes thermodynamically unstable and phase separation occurs into a polymer rich and a polymer lean phase. The concentrated phase solidifies shortly after phase separation and forms the matrix, whereas the polymer lean phase forms the pores. A phase diagram coupled with thermodynamic and kinetic aspects provides information about structure formation in membranes. All these general aspects may be transferable to the formation of porous polymer fibers.

Another mechanism to be considered in the formation of porous electrospun fibers is that of breath figures recently described by Srinivasarao et al. Breath figures occur as a result of evaporative cooling due to rapid solvent evaporation therefore significantly cooling the surface of the electrospinning jet as it travels from the syringe to the target. As the surface cools moisture in the air condenses and grows in the form of droplets. The droplets remain as individual entities acting as hard spheres due to convection currents on the surface of the jet. As the jet dries, leaving dried fibers, the water droplets leave an imprint on the surface of the fibers in the form of pores.[1] Preliminary studies have shown that humidity does play a role on the formation of porous electrospun fibers as shown in Figure 10, and therefore, this mechanism may play a dominate role in describing how and why pores form of these fibers.

However most of the literature describes very uniform circular densely packed pore formation as the result of breath figures.[9,40] As indicated throughout this paper we observe a variety of structures on the fiber surfaces from densely packed irregular shaped pores (PS/THF)

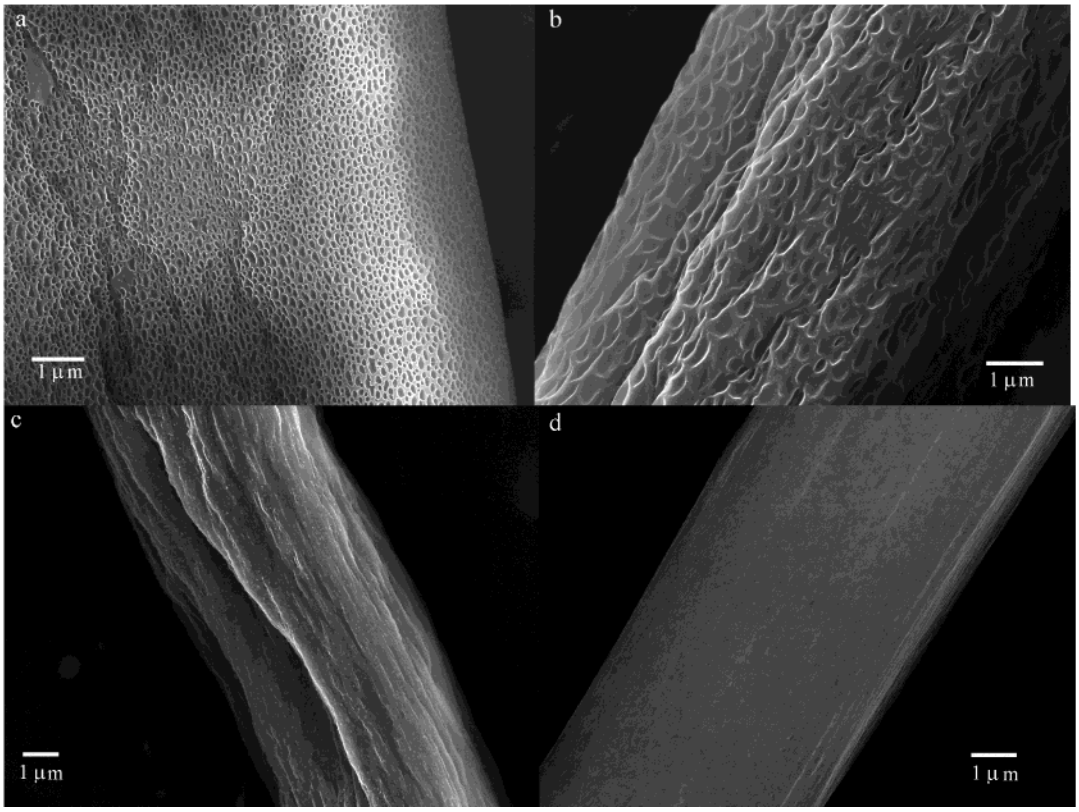

Figure 7. FESEM images of PS fibers as a function of solution volatility: (a) 100% THF (15 kV, WD 8.9 mm); (b) 75/25% THF/DMF (15 kV, WD 9.3 mm); (c) 50/50% THF/DMF (15 kV, WD 8.8 mm); (d) 100% DMF (15 kV, WD 9.0 mm).

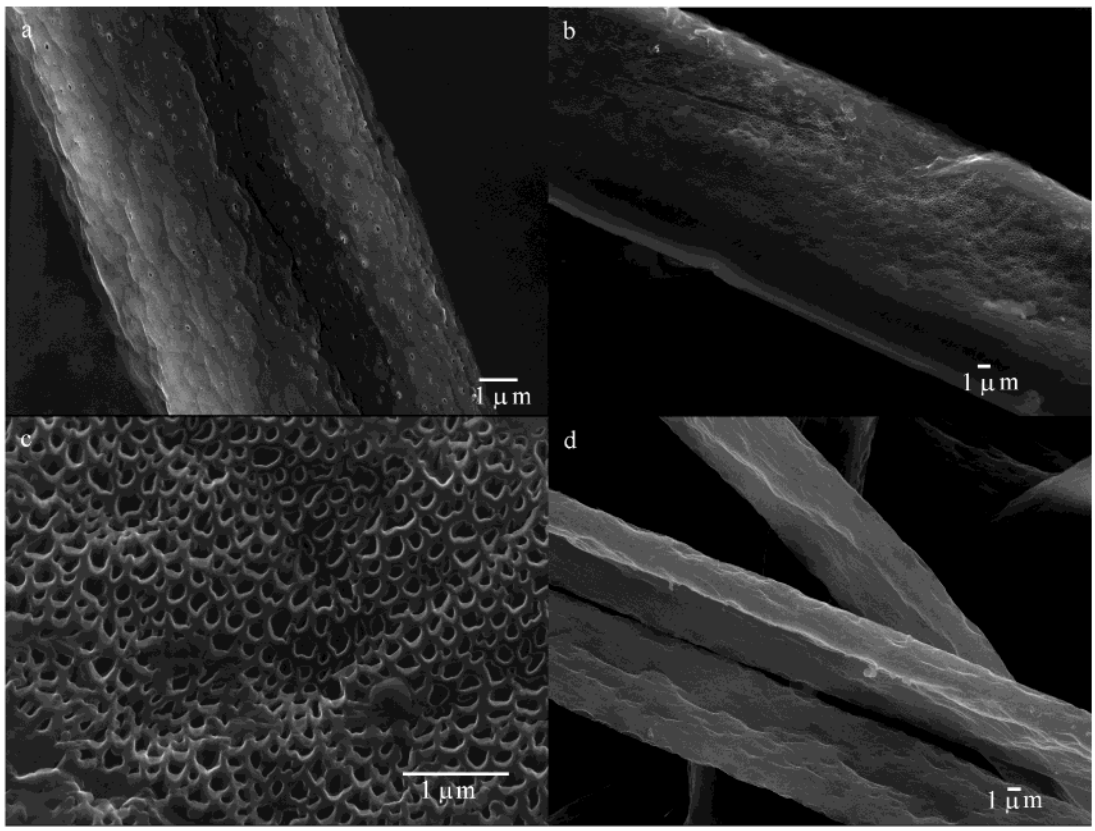

Figure 8. FESEM images of PMMA fibers electrospun from (a) acetone, (b) $CHCl_3$, (c) larger magnification of part b (a,b,c: 15 kV, WD 4.8 mm), and (d) THF (15 kV, WD 4.5 mm). In all cases, 10 wt % PMMA solutions were used; for conditions, see Table 3.

to extremely rough surfaces with loosely packed elongated pores (PMMA/acetone). These differences may arise because of variations in experimental conditions between these experiments and traditional breath figure

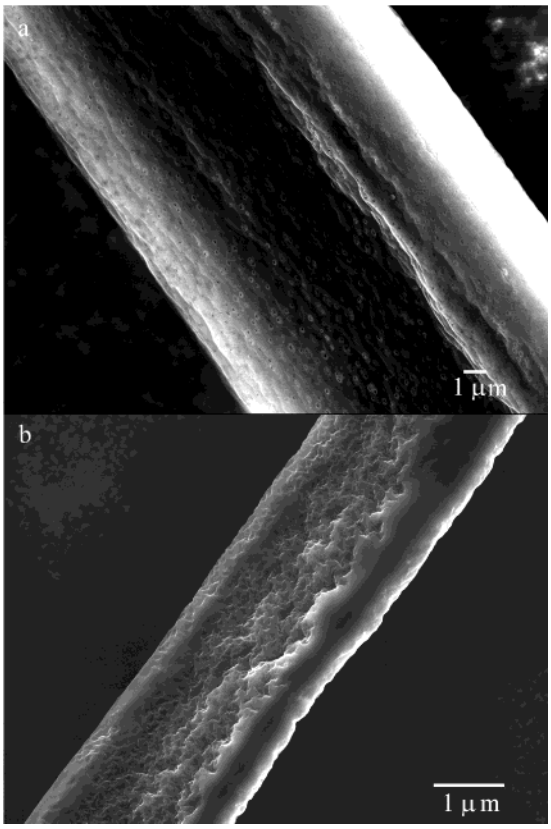

Figure 9. FESEM images of PC fibers electrospun from (a) $CHCl_3$ and (b) THF (15 kV, WD 4.5 mm).

experiments. For example in the electrospinning process the concentrated polymer solution is accelerated through the humid air whereas in the work by Srinivasarao et al. the humid air is moving across the surface of the solution.[1] Due to these differences, phase separation mechanisms must also be considered in the explanation of pore formation of electrospun fibers.

A. Thermally Induced Phase Separation (TIPS). Phase separation occurs by lowering the temperature of the solution in TIPS. The solution then passes through the binodal curve of the phase diagram to enter the metastable region. Amorphous polymers are known to produce microporous structures by liquid/liquid phase separation, which is followed by the gelation of the polymer.[41] Microporous structure formation has been observed in semicrystalline polymers due to combined crystallization and liquid/liquid phase separation.[42]

Although the temperature was kept constant during the electrospinning process, evaporative cooling occurs as the fiber traverses the distance between the syringe and the target. This could cause TIPS during fiber formation. If the evaporative cooling affects only the temperature of the fiber surface, this might explain the occurrence of pores on the surface only. At this point it is not known whether the temperature is changed along the cross section of the fiber. Measurements of temperature differences along the fiber during electrospinning with an ultrafast heat sensitive camera would provide additional information but is beyond the scope of the current investigation.

PS and PMMA are amorphous polymers, whereas PEO and PC are semicrystalline. This could effect some differences in the surface morphology of the investigated materials when TIPS occurs. Also as indicated earlier, the T_g of these polymers varies from −67 (PEO) to +150 °C (PC), and thus plasticization of the PC fibers could effect the pore formation and, as the solvent evaporates, be responsible for freezing in the porous surface morphology.

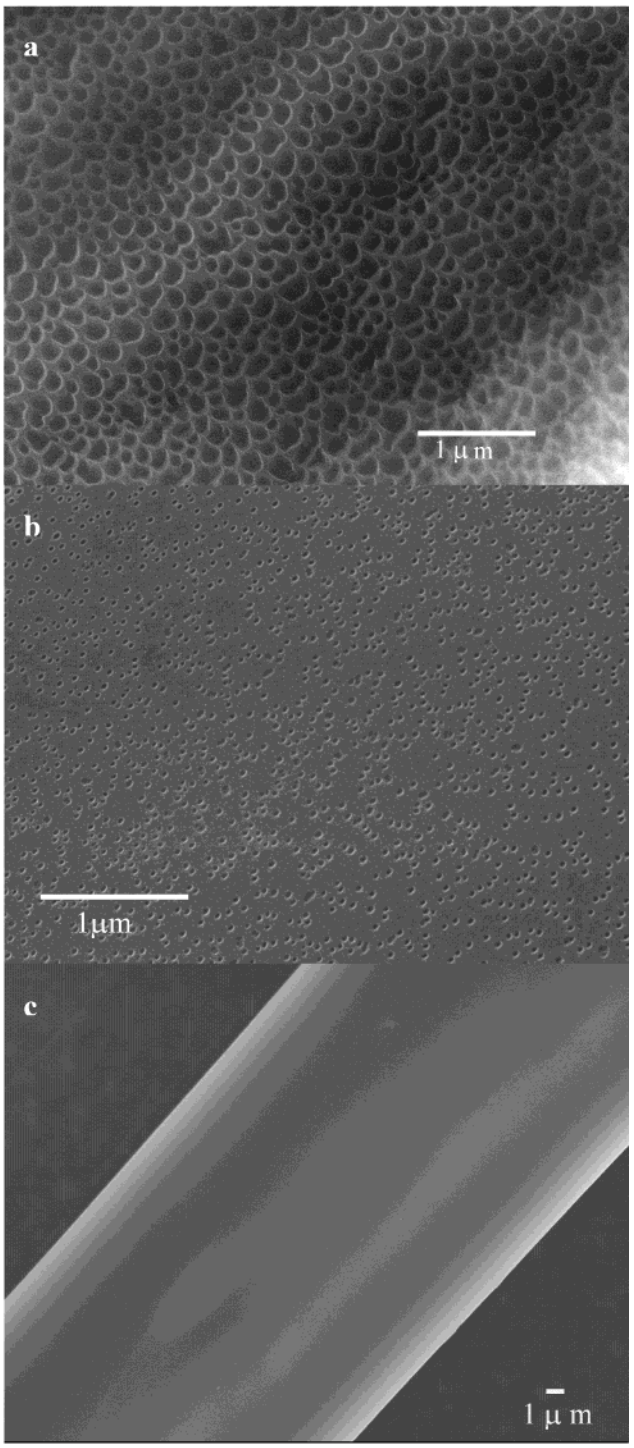

Figure 10. FESEM images of PS fibers electrospun from THF (35 wt % PS/THF) at different relative humidities: (a) 50% relative humidity (15 kV, WD 5.5 mm), (b) 30% relative humidity (15 kV, WD 6.7 mm), and (c) 20% relative humidity (15 kV, WD 5.8 mm).

B. Vapor-Induced Phase Separation. During vapor-induced phase separation the polymer solution undergoes phase separation by penetration of nonsolvent from the vapor phase. Since the mass transfer is very slow, only a flat concentration profile is obtained in the membrane. The rate-limiting step for the nonsolvent

transport into the polymer solution is the slow diffusion in the vapor phase adjacent to the film surface.[43] If the vapor phase is saturated with solvent, skin formation can be hindered, which is possible for high volatile solvents. In this case, the pore formation is determined by the vapor pressure of the nonsolvent and the polymer concentration. Increasing relative humidity or decreasing polymer concentration would increase the pore formation.

In addition to condensing on the fiber surface due to evaporative cooling, water in the atmosphere also works as a nonsolvent for all investigated polymers, except for PEO. This might also contribute to some of the differences in surface morphology observed when PS fibers are electrospun from THF at different relative humidities. We have also observed that the pore formation is clearly decreased with increasing PMMA concentration from 10 to 30 wt % in an experiment where different PMMA concentrations were electrospun from THF. This might also reflect an effect of vapor-induced phase separation. The occurrence of pores only on the fiber surfaces also supports vapor-induced phase separation rather than a TIPS process.

Conclusion

This work describes investigations on four different polymers electrospun from various solvents to create a broad range of fibers with different surface morphologies. The ability to produce polymeric fibers or materials with a tailorable surface morphology increases their range of application significantly. When a nanoporous morphology, as shown in these studies, is combined with the exceptionally small diameters (10−1000 nm) of the smallest fibers, it can give rise to an extremely large surface area (∼100−1000 m^2/g). The surface area of these small fibers can easily surpass that of silica gel (400 m^2/g) if a nanoporous texture is added. This property makes them ideal candidates for cell adhesion, catalysis, filter, and fuel cell membrane applications.

The process of pore formation arising from rapid solvent evaporation most likely occurs due to the formation of water droplets from atmospheric water due to evaporative cooling of the polymer solution as they travel the distance from the syringe to the target. Currently, it is clear that the solvent vapor pressure has a critical influence on the process of pore formation. TEM measurements of a cross section of PS fibers clearly indicated that the pores appear only on the surface of the fibers, which are known to be dry when they reach the target.[11]

Solvent diffusion in polymers plays an important role in the evaporation process as already mentioned. The diffusion coefficients of the solvents and the solubility parameters of the polymers and of the solvents as well as the interaction parameters between polymer and solvent are parameters of influence. More detailed investigations need to be done in order to take more specific polymer and solvent properties into consideration. However, there are many more solvent and polymer properties including electrical and thermal effects that also need to be considered for a complete description of this complex electrospinning process.

Acknowledgment. The authors would like to acknowledge partial support for this work from NSF (DMR-9812088 and DMR-0210223) and DOE PAIR. We also want to thank Nancy Tassi for her insight and expertise in SEM, TEM, and AFM, Gerald Poirier for his FESEM expertise in imaging the nanoporous fibers, Dr. Darrin Pochan and Dr. Chou Ni for preparing the microtomed samples and doing the TEM measurements, Beth Schubert for performing the viscosity measurements, and Dr. Mei Wei Tsao and Dr. Richard Ikeda for the many helpful discussions.

References and Notes

(1) Srinivasarao, M.; Collings, D.; Philips, A.; Patel, S. *Science* **2001**, *292*, 79.
(2) Gao, C.; Li, A.; Feng, L.; Yi, X.; Shen, J. *Polym. Int.* **2000**, *49*, 323.
(3) Gao, C.; Li, A.; Yi, X.; Shen, J. *J. Appl. Polym. Sci.* **2001**, *81*, 3523.
(4) Strathmann, H. Synthetic membranes and their preparation. In *Synthetic Membranes: Science, Engineering and Applications*; Bungay, P. M., et al., Eds.; D. Reidel Publishing Co.: Dordrecht, The Netherlands, 1984; pp 1−37.
(5) Van de Witte, P.; Dijkstra, P. J.; Van den Berg, J. W. A.; Feijen, J. *J. Membr. Sci.* **1996**, *117*, 1.
(6) Gibson, P.; Schreuder-Gibson, H.; Rivin, D. *Colloids Surf. A* **2001**, 187−188, 469.
(7) Bognitzki, M.; Czado, W.; Frese, T.; Schaper, A.; Hellweg, M.; Steinhart, M.; Greiner, A.; Wendorff, J. H. *Adv. Mater.* **2001**, *13*, 70.
(8) Bognitzki, M.; Frese, T.; Steinhart, M.; Greiner, A.; Wendorff, J. H.; Schaper, A.; Hellweg, M. *Polym. Eng. Sci.* **2001**, *41*, 982.
(9) Reneker, D. H.; Chun, I. *Nanotechnology* **1996**, *7*, 216.
(10) Liu, W.; Wu, Z.; Reneker, D. H. *Polym. Prepr.* **2000**, *41*, 1193.
(11) Stephens, J. Private communication, 2001.
(12) Warner, S. B.; Buer, A.; Grimler, M.; Ugbolue, S. C.; Rutledge, G. C.; Shin, M. Y. *Natl. Text. Cent. Annu. Rep.* **1999.**
(13) Berghoef, M. M.; Vansco, J. G. *Adv. Mater.* **1999**, *11*, 1362.
(14) Fong, H.; Reneker, D. H. *J. Polym. Sci. B* **1999**, *37*, 3488.
(15) Buchko, C. J.; Chen, L. C.; Shen, Y.; Martin, D. C. *Polymer* **1999**, *40*, 7397.
(16) Huang, L.; McMillan, A.; Apkarian, R. P.; Pourdeyhimi, B.; Conticello, V. P.; Chaikof, E. L. *Macromolecules* **2000**, *33*, 2989.
(17) Norris, I. D.; Shaker, M. M.; Ko, F. K.; MacDiarmid, A. G. *Synth. Met.* **2000**, *114*, 109.
(18) Gibson, P.; Schreuder-Gibson, H. *Porous, Cellular and Microcellular Materials*; MD-Vol. 91, ASME: Fairfield, NJ, 2000; p 45.
(19) Bognitzki, M.; Hou, H.; Ishaque, M.; Frese, T.; Hellweg, M.; Schwarte, C.; Schaper, A.; Wendorff, J. H.; Greiner, A. *Adv. Mater.* **2000**, *12*, 637.
(20) Mac Diarmid, A. G.; Jones, W. E.; Norris, I. D.; Gao, J.; Johnson, A. T.; Pinto, N. J.; Hone, J.; Han, B.; Ko, F. K.; Okuzaki, H.; Llaguno, M. *Synth. Met.* **2001**, *119*, 27.
(21) Fong, H.; Weidong, L.; Wang, C. S.; Vaia, R. A. *Polymer* **2002**, *43*, 775.
(22) Formhals, A. Process and apparatus for preparing artificial threads. US Patent 1,975,504, 1934.
(23) Baumgarten, P. K. *J. Colloid Interface Sci.* **1971**, *36*, 71.
(24) Hohman, M. M.; Shin, M.; Rutledge, G.; Brenner, M. P. *Phys. Fluids* **2001**, *13*, 2201.
(25) Hohman, M. M.; Shin, M.; Rutledge, G.; Brenner, M. P. *Phys. Fluids* **2001**, *13*, 2221.
(26) Yarin, A. L.; Koombhongse, S.; Reneker, D. H. *J. Appl. Phys.* **2001**, *89*, 3018.
(27) Reneker, D. H.; Yarin, A. L.; Fong, H.; Koombhongse, S. *J. Appl. Phys.* **2000**, *87*, 4531.
(28) Spivak, A. F.; Dzenis, Y. A.; Reneker, D. H. *Mech. Res. Commun.* **2000**, *27*, 37.
(29) Rutledge, G. C.; Li, Y.; Fridrikh, S.; Warner, S. B.; Kalayci, V. E.; Patra, P. *Natl. Text. Cent. Annu. Rep.* **2001**, *Nov.*, M01-D22.
(30) Theron, A.; Zussman, E.; Yarin, A. L. *Nanotechnology* **2001**, *12*, 384.
(31) Deitzel, J. M.; Kleinmeyer, J.; Harris, D.; Beck Tan, N. C. *Polymer* **2001**, *42*, 261.
(32) Billmeyer, F. W. *Textbook of Polymer Science*, 2nd ed.; John Wiley & Sons: 1971; pp 410, 439.
(33) Shin, M.; Hohman, M. M.; Brenner, M. P.; Rutledge, G. *Appl. Phys. Lett.* **2001**, *78*, 1149.

(34) Fong, H.; Chun, I.; Reneker, D. H. *Polymer* **1999**, *40*, 4585.
(35) Doshi, J.; Reneker, D. H. *J. Electrost.* **1995**, *35*, 151.
(36) Park, H. C.; Kim, Y. P.; Kim, H. Y.; Kang, S. Y. *J. Membr. Sci.* **1999**, *156*, 169.
(37) Matsuyama, H.; Teramoto, M.; Nakatani, R.; Maki, T. *J. Appl. Polym. Sci.* **1999**, *74*, 171.
(38) Beltsios, K.; Athanasiou, E.; Aidinis, C.; Kanellopoulos, N. *J. Macromol. Sci.—Phys. B* **1999**, *38*, 1.
(39) Wijmans, J. G.; Smolders, C. A. Preparation of asymmetric membranes by the phase inversion process. In *Synthetic Membranes: Science, Engineering and Applications*; Bungay, P. M., et al., Eds.; D. Reidel: Publishing Co: Dordrecht, The Netherlands, 1984; p 39.
(40) Limaye, A. V.; Narhe, R. D.; Dhote, A. M.; Ogale, S. B. *Phys. Rev. Lett.* **1996**, *76*, 3762.
(41) Laxminarayan, A.; McGuire, K. S.; Kim, S. S.; Lloyd, D. R. *Polymer* **1994**, *35*, 3060.
(42) Caneba, G. T.; Soong, D. S. *Macromolecules* **1985**, *18*, 2545.
(43) Strathmann, H. Production of microporous media by phase inversion process. In *Material Science of Synthetic Membranes*; Lloyd, D. R., Eds.; ACS Symposium Series 269; American Chemical Society: Washington, DC, 1985; pp 165—195.
(44) Koombhongse, S.; Liu, W.; Reneker, D. H. *J. Polym. Sci., Part B: Polym. Phys.* **2001**, *39*, 2598.

MA020444A